



Delft University of Technology

Numerical prediction on abrasive wear reduction of bulk solids handling equipment using bionic design

Chen, Guangming; Lodewijks, Gabriel; Schott, Dingena L.

DOI

[10.1080/02726351.2018.1480547](https://doi.org/10.1080/02726351.2018.1480547)

Publication date

2018

Document Version

Final published version

Published in

Particulate Science and Technology

Citation (APA)

Chen, G., Lodewijks, G., & Schott, D. L. (2018). Numerical prediction on abrasive wear reduction of bulk solids handling equipment using bionic design. *Particulate Science and Technology*, 37 (2019)(8), 960-969.
<https://doi.org/10.1080/02726351.2018.1480547>

Important note

To cite this publication, please use the final published version (if applicable).

Please check the document version above.

Copyright

Other than for strictly personal use, it is not permitted to download, forward or distribute the text or part of it, without the consent of the author(s) and/or copyright holder(s), unless the work is under an open content license such as Creative Commons.

Takedown policy

Please contact us and provide details if you believe this document breaches copyrights.

We will remove access to the work immediately and investigate your claim.



Particulate Science and Technology

An International Journal

ISSN: 0272-6351 (Print) 1548-0046 (Online) Journal homepage: <https://www.tandfonline.com/loi/upst20>

Numerical prediction on abrasive wear reduction of bulk solids handling equipment using bionic design

Guangming Chen, Gabriel Lodewijks & Dingena L. Schott

To cite this article: Guangming Chen, Gabriel Lodewijks & Dingena L. Schott (2019) Numerical prediction on abrasive wear reduction of bulk solids handling equipment using bionic design, *Particulate Science and Technology*, 37:8, 964-973, DOI: [10.1080/02726351.2018.1480547](https://doi.org/10.1080/02726351.2018.1480547)

To link to this article: <https://doi.org/10.1080/02726351.2018.1480547>



Published online: 17 Aug 2018.



Submit your article to this journal 



Article views: 137



View related articles 



View Crossmark data 

Numerical prediction on abrasive wear reduction of bulk solids handling equipment using bionic design

Guangming Chen^{a,b}, Gabriel Lodewijks^{b,c} , and Dingena L. Schott^b

^aInstitute of Bio-inspired Structure and Surface Engineering, Nanjing University of Aeronautics and Astronautics, Nanjing, China; ^bDepartment of Maritime and Transport Technology, Delft University of Technology, Delft, The Netherlands; ^cSchool of Aviation, The University of New South Wales, Sydney, NSW, Australia

ABSTRACT

Abrasive wear can cause surface damage of bulk solids handling equipment. Reducing the abrasive wear is beneficial to lower the maintenance cost. Previous research elaborated on the bionic design methodology to reduce surface wear of bulk solids handling equipment. To facilitate the application of the bionic design methodology in bulk solids handling, this research examines the effectiveness of a bionic model using discrete element method (DEM) simulations. A reference case of an abrasive wear scenario in bulk solids handling is simulated, and the wear volume of a smooth chute surface is predicted. By applying a bionic model to the chute surface and using the same simulation model, the wear volume of a bionic surface is predicted. By comparisons, it is identified that the bionic surfaces produce less wear than the smooth surface. In addition, the sensitivities of the geometrical parameters for the wear reduction are predicted. Therefore, the abrasive wear reduction effectiveness of the bionic model is demonstrated.

KEYWORDS

Bionic surface; bulk solid; discrete element method; particle flow; sliding wear

1. Introduction

Bulk solids handling plays an important role in a wide range of industries, such as the agricultural, chemical and mining industries. In the mining industry, for example, the iron ore bulk solid is exploited intensively to supply the base material for steel products. During the handling of iron ore, the handling equipment surfaces (e.g. chute bottom) can suffer from severe abrasive wear (Roberts 2003; Hilgraf 2007). The abrasive wear decreases the thickness of wearing equipment surface and thus accelerates surface damage.

Currently, several methods are utilized to reduce abrasive wear. For instance, optimizing chute profile design based on theoretical evaluations (Roberts 2003). Besides, wear-resistant materials are applied on wearing surfaces (Hilgraf 2007). However, using these traditional methods still results in excessive wear. Bionic design [or biomimetic design (Sartori, Pal, and Chakrabarti 2010), bio-inspired design (Vincent 2009)] is an innovative method which can transfer biological mechanisms to industrial design (Malshe et al. 2013; Müller, Kunz, and Gräf 2016). In order to achieve further wear reduction of bulk solids handling equipment, the bionic design method has been introduced (Chen, Schott, and Lodewijks 2017b). Moreover, a bionic model for abrasive wear reduction of bulk solids handling equipment surface was proposed (Chen, Schott, and Lodewijks 2017b). Nonetheless, the effectiveness of applying this model for wear reduction under bulk solids handling conditions is not yet demonstrated.

The object of this paper is to demonstrate the effectiveness of using the bionic model (Chen, Schott, and Lodewijks 2017b) for the abrasive wear reduction of bulk solids handling equipment surfaces. In bulk solids handling industry, the Sishen iron ore is highly demanded and many pieces of handling equipment are made of mild steel. Accordingly, the abrasive wear of mild steel surface by the Sishen iron ore is modeled with the reference of bulk solids handling conditions.

To model interactions of such particulate system, the discrete element method (DEM) is generally used on account of its reliance and accuracy (Cundall and Strack 1979; Khanal and Morrison 2009; Tang, Zhang, and Ji 2017). By implementing appropriate contact model (Popov 2010; DEM Solutions Ltd. 2016a) and wear equations, although the actual surface shapes subjected to wear evolution cannot be modeled, the wear volumes of geometry can be predicted (Boemer and Ponthot 2017). Accordingly, a constant wear rate (coefficient of sliding wear) can be used for predicting wear volumes. This simulation research employs Archard's wear model (Archard 1953; Chen, Schott, and Lodewijks 2017a) to predict wear volumes using the software EDEM® 2.7 (DEM Solutions Ltd. 2016b) and application programming interface (API).

The organization of this paper is given as follows. Section 2 describes the referential setup for abrasive wear modeling; Section 3 presents the determinations of DEM parameters; Section 4 illustrates the abrasive wear prediction of a smooth surface; Section 5 provides the abrasive wear prediction of bionic surfaces; Section 6 presents the sensitivity analysis

of the bionic model. Finally, the conclusions are given in Section 7.

2. Referential setup for abrasive wear modeling

Figure 1(a) illustrates the setup of a part of bulk solids handling process that is using a belt conveying system. This transfer process relies upon three items: namely, the feeder, chute and conveyor. The cross-section of this curved chute is constant. Under rapid flow conditions (Roberts 2003), severe abrasive wear occurs on the chute bottom surface. Figure 1(b) shows the flow model corresponding to rapid flow condition.

To efficiently model the wear process from the perspective of saving computational cost, the number of modeled particles must be reduced. Therefore, in comparison with practical setup, the modeled width of feeder and chute is reduced. The capacity is reduced to 100 t/h (27.78 kg/s) and the modeled feeder speed is limited at 0.2 m/s. This does not affect the simulation of bulk flow based on our tests of angle of repose ([Section 3.5](#)). To further reduce simulation time, the conveyor is not modeled since it has no influence on the simulated wear. [Table 1](#) summarizes the determined values for the dimension and position parameters in [Figure 1](#).

In addition to the determinations for the dimensions and positions, Figure 1 shows that two angles must also be determined. The first angle γ is determined at 45° referring to the setup in Roberts (2003). The second angle Ψ (the cut-off angle) is approximated at 30° by relating to wall friction angle θ_w , i.e. $\Psi \approx \theta_w + 5^\circ$. For the condition of the Sishen iron ore handling, the wall friction angle θ_w is measured at around 25° . Note that a full list of used symbols are represented in the Nomenclature section.

3. Determination of DEM parameters

Section 2 introduced the referential setup for modeling abrasive wear. In this section, a group of DEM parameters

values are determined to predict wear in bulk solids handing. Firstly, all DEM parameters are analyzed from the four categories: namely, the particle, geometry, contact and simulation parameters. After the analysis of the parameters, angle of repose tests (Lumay et al. 2012) are carried out to obtain a group of DEM parameter values for modeling bulk flow.

3.1. Particle parameters

The particle parameters include particle size (diameter), density, Poisson's ratio and shear modulus. The particle sizes of the Sishen iron ore sample are 0–18 mm (Chen et al. 2017). However, in simulations the sizes are 3–8 mm, which eliminates the particles whose sizes are less than 3 mm. The purpose of doing so is that the computational time can be significantly reduced due to the significant reduction of particle numbers. To ensure that the simulated particle sizes can correctly resemble the bulk flow behavior as in practice, the calibration test of angle of repose is conducted (Section 3.5). The average particle density was measured at $4865 \pm 72 \text{ kg/m}^3$ (using 95% confidence interval) by a gas-expansion pycnometer. The adopted Poisson ratio and shear modulus are based on the research in (Chen, Schott, and Lodewijks 2017a), which are 0.24 and 65 GPa.

3.2. Geometry parameters

The geometry parameters are composed of density, Poisson's ratio, shear modulus, rotating speed and mesh size. As mentioned in the “Introduction” section, mild steel is used as geometry of chute surface material. The determinations of density, Poisson's ratio and shear modulus of the mild steel surface are stated in the previous work (Chen, Schott, and Lodewijks 2017a), which are 7932 kg/m^3 , 0.3 and 78 GPa.

Table 1. Dimensions and positions of the transfer setup.

Denotations	B_1	B_c	h_1	h_2	h_3	h_4	l_1	l_2	R_0	R_1	s_1	s_2
Values (m)	0.3	0.2	0.5	0.3	1.8	0.4	0.5	0.25	0.2	2.0	0.2	0.2

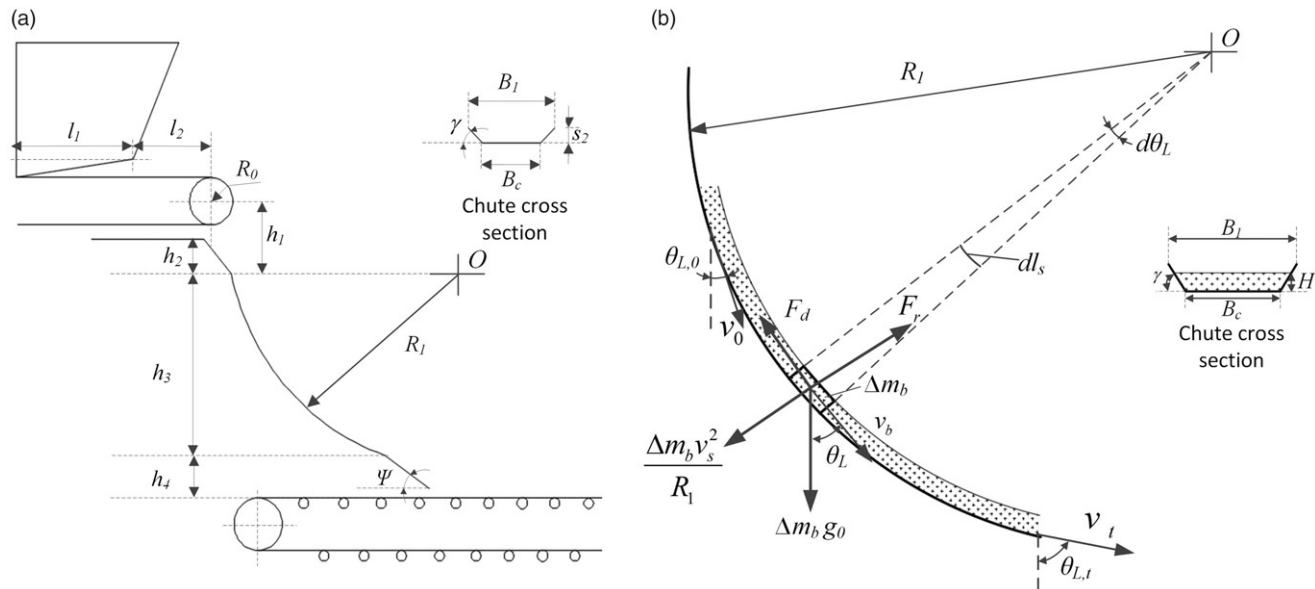


Figure 1. A transfer process in a belt conveying system (a); referred setup (b) analytical model of chute flow (Roberts 2003)

For the mesh size of the chute geometry, the ANSYS Workbench 16.2 (ANSYS Inc. 2016) is applied and the setting preferences are: CFD-Fluent, high smooth sizing. To achieve realistic distribution of wear, the mesh size must be significantly small (Chen, Schott, and Lodewijks 2017a). Meanwhile, considering the computational cost which is proportional to the number of meshes, the maximal mesh size is set at 6 mm. At this size, the number of meshes is not too large whilst realistic distribution of wear is obtained.

3.3. Contact parameters

To model the wear process on the chute, two types of contacts are considered: namely, particle/particle and particle/geometry. The preliminarily determined parameter values for iron ore/iron ore contact are based on our laboratory tests and available research (Barrios et al. 2013): the used coefficient of restitution is 0.45; the coefficient of static friction is estimated between 0.4 and 0.6 and the coefficient of rolling friction is between 0.1 and 0.3 (DEM Solutions Ltd. 2016a).

For iron ore/chute contact, the coefficient of restitution is estimated at 0.4 (Barrios et al. 2013). The applied value of the coefficient of static friction is 0.46 based on our experimental tests (Chen et al. 2017). The coefficient of rolling friction is estimated between 0.2 and 0.4 (Barrios et al. 2013) referring to experiments of using spherical particles.

3.4. Simulation parameters

This simulation includes the six parameters: namely, particle generation rate, initial horizontal velocity, initial vertical velocity, coefficient of sliding wear, total time and time step. In EDEM® (DEM Solutions Ltd. 2016b), a particle factory is utilized to generate bulk solids with specific flow rate and velocities. The total time is selected at 4.0 s at which time a steady transportation is reached. Using the particle factory, the transport capacity is assigned to be 27.78 kg/s. Using the determined values in Table 1 and neglecting air resistance, the horizontal velocity of bulk solids at the onset of contact with respect to chute bottom is calculated as $v_{x,0} = 0.20 \text{ m/s}$. The vertical velocity $v_{y,0} = -5.33 \text{ m/s}$ is calculated using Equation (1).

$$v_{y,0} = \sqrt{v_{x,0}^2 + \frac{g_0^2(h_1 + r_1)^2}{v_{x,0}^2}} \quad (1)$$

During the handling of bulk solids on chute bottom surface, the particles can have both sliding and rolling motions, which can be resembled using DEM simulations. However, in this research, the abrasive wear caused by particle rolling is not accounted for because it makes minor contribution in comparison with the total wear (Hilgraf 2007). Thus, total abrasive wear is quantified solely from particle sliding. To estimate sliding wear, the previous work (Chen, Schott, and Lodewijks 2017a) demonstrated that Equation (2) which was derived based on Archard's wear model (Archard 1953) can be used,

$$W_V = \alpha_s \sum_0^i \left[\left(-\frac{2}{3} S_n \delta_n^{1/2} + C_n v_n \right) l_s \right] \quad (2)$$

where α_s is the coefficient of sliding wear; i is the number of wear events on the geometry subjected to particle contacts; S_n is the coefficient of normal stiffness; δ_n is the normal overlap between the particle and equipment surface; C_n is the coefficient of damping force; v_n is the normal velocity of particle relative to equipment and l_s is the sliding distance made on the geometry surface meshes (Powell et al. 2011; Chen, Schott, and Lodewijks 2017a).

For the used coefficient of sliding wear $\alpha_{s,e}$ it is assumed to be a constant during whole wear processes. Here it is set at $3.0 \times 10^{-13} \text{ m}^2/\text{N}$ referring to our experimental measurement (Chen et al. 2017). The determined time step is $1.5 \times 10^{-6} \text{ s}$, which was estimated in the previous work (Chen, Schott, and Lodewijks 2017a).

3.5. Angle of repose

To find out a group of DEM parameter values for modeling bulk solids, the coefficients of static friction and rolling friction for particle/particle, and the coefficient of rolling friction for particle/geometry must be specified. To do so, angle of repose as calibration test can be used (Lumay et al. 2012).

The experimental setup to perform angle of repose test is designed as shown in Figure 2(a). The box is fed with the Sishen iron ore sample. To start a test, the front sheet is quickly rotated upwards to release the bulk solids. Synchronously, the loaded bottom surface is initiated by applying an angular speed ω . A bin with a steel bottom surface is used to restore the bulk solids, the same sample is reused for next tests. During the tests, two rotating speeds are employed within the adjustable speed range of this tester: namely, $1.8^\circ/\text{s}$ and $13.1^\circ/\text{s}$. To obtain stable values of the angles of repose, the tests are repeated eight times with respect to each speed. In order to model the test of angle of repose, the used values for DEM parameters are discussed in the following text.

The used values for particle parameters are stated in Section 3.1. For the geometry parameters, acrylic sheets are used to construct the feeder for storing the iron ore. Besides, two steel sheets are modeled respectively to simulate the surface of rotational plane and the bin bottom. The acrylic sheet and the inclining surface can be directly created using the basic polygons in EDEM® (DEM Solutions Ltd. 2016b). The density, Poisson's ratio and shear modulus of the modeled acrylic sheet are 1136 kg/m^3 , 0.4 and 11 GPa (Grima and Wypych 2011; SCRIBD 2017).

For the contact parameters, an additional contact which is iron ore and acrylic sheet is introduced because a new material of acrylic sheet is implemented. Based on the available resources (Grima and Wypych 2011; SCRIBD 2017), the corresponding values for the coefficients of restitution, static friction and rolling friction are estimated, which are 0.5, 0.24 and 0.22.

For the simulation parameters, periodic boundary (DEM Solutions Ltd. 2016b) is adopted to reduce the modeled domain and thus enabling further reduction of simulation time based on the critical ratio of domain width to particle size ($Z_s/d_p > 4$) (Derakhshani, Schott, and Lodewijks 2016). A particle factory is used to generate bulk solid particles

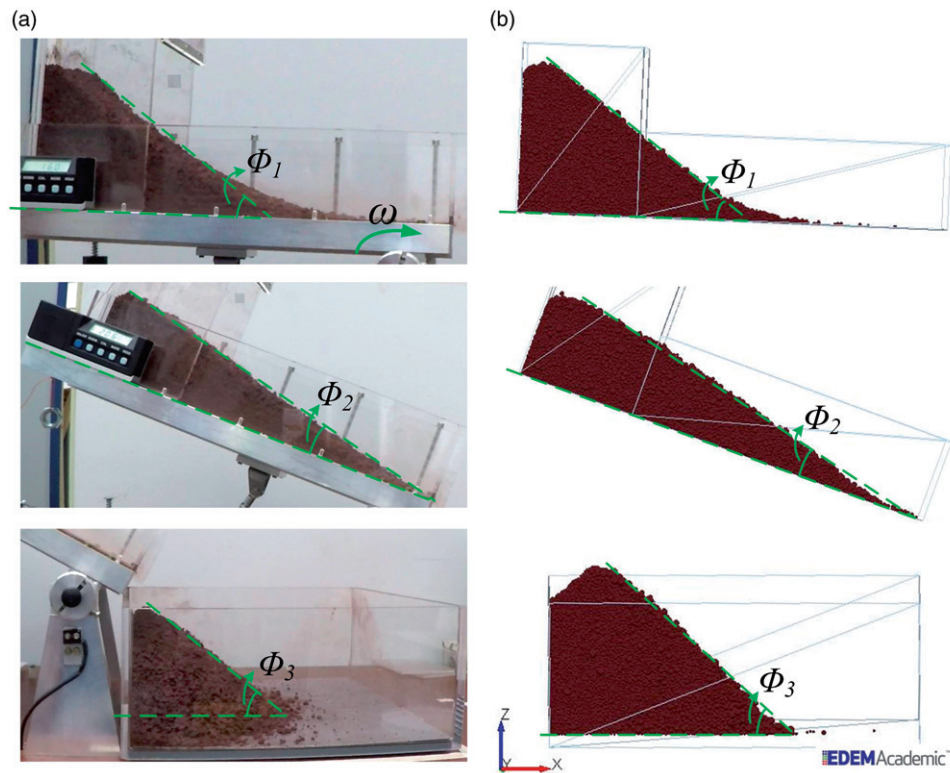


Figure 2. Modeling iron ore bulk flow behaviour (a) a test from Experiment 1; (b) a test from Simulation 1.

with specific mass rate, total time and initial velocities as those of experimental levels. In simulations, the particle generation rate is set at 1.5 kg/s and the total time is 1.85 s. The particle feeding velocity is 1.0 m/s. Based on preliminary simulations, huge simulation time is required to model a full process of bulk solids flowing over the inclining surface. Thus, a compromise between the simulation time and simulation accuracy has to be made. In this research, the simulation speeds are increased to 10 times (i.e. $1.8^\circ/\text{s}$ and $13.1^\circ/\text{s}$) of the laboratory speeds. By so doing, the simulation time can be significantly reduced while maintaining the bulk flow characteristics in the laboratory test. Using the same time step as previously determined, all values for the simulation parameters are obtained.

Figure 2 shows three snapshots from a test in Experiment 1 and a test in Simulation 1. By comparing the three angles (Φ_1 , Φ_2 and Φ_3), it demonstrates that the simulated bulk flow maintains high similarities with those of the experiments. Based on three repetitive simulations, it is obtained that the simulation predictions are stable. Nevertheless, it must be noted that after all particles have fallen into the bin, the particles of the bulk pile (the bottom row in Figure 2) still maintain a very slow horizontal motion due to low resistance between particles and bin bottom. In practice, the bulk pile reaches steady state instantly owing to much high sliding resistance generated by non-spherical particles. This indicates that using spherical particles brings about particle movements with respect to the contact geometry. In this simulation, angle Φ_3 is selected when the kinetic energy of total particles arrives at a low value of $1.8 \times 10^{-5} \text{ J}$.

Using the trial-and-error method, the tests of angle of repose for both low and high speeds are modeled based on

Table 2. Comparisons of the three angles obtained by experiments and simulation.

Groups	Angle 1, Φ_1 [°]	Angle 2, Φ_2 [°]	Angle 3, Φ_3 [°]
Experiment 1	33.8 ± 0.7	35.6 ± 1.2	38.9 ± 1.1
Simulation 1	35.4 ± 0.2	35.4 ± 0.7	42.4 ± 1.4
Experiment 2	33.7 ± 0.9	37.7 ± 0.7	33.3 ± 0.8
Simulation 2	32.7 ± 0.6	37.8 ± 0.4	33.8 ± 0.9

the significantly equivalent angles (Φ_1 , Φ_2 and Φ_3) from experiments and simulations (Table 2). The error ranges for the angles are obtained using 95% confidence interval. It is seen that, although the angle Φ_3 in the Simulation 1 falls outside the range of experimental results, the other angles from the simulations lie in experimental values. Thus far, a group of values for the DEM simulation have been found out to model the flow behaviour for iron ore bulk solids, which are given in Table 3.

4. Abrasive wear prediction of smooth surface

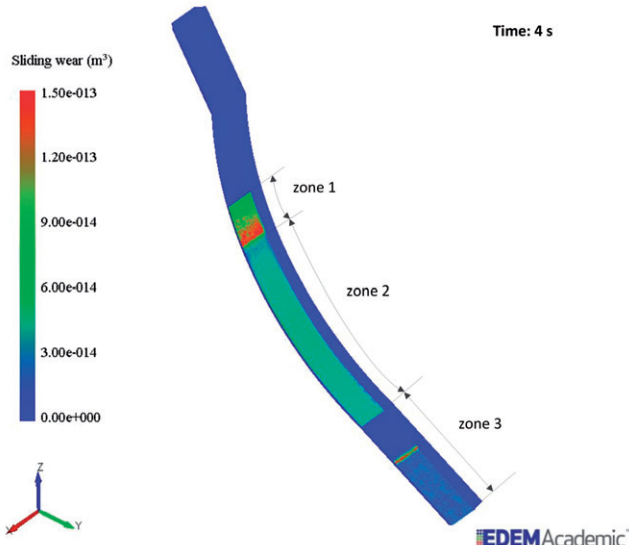
Using wear prediction model (Equation (2)) and the determined DEM values (Table 3), the abrasive wear for the iron ore handling conditions can be predicted using the software EDEM® 2.7 (DEM Solutions Ltd. 2016b). This section illustrates the DEM prediction of the abrasive wear on the smooth surface of the chute. Furthermore, the theoretical verification of the abrasive wear prediction is provided.

4.1. Abrasive wear prediction by DEM

To efficiently model wear process using DEM simulation, the geometry sizes of the particle factory are adjusted: the

Table 3. Values for modeling abrasive wear on the chute.

Category	Wear aspect	DEM parameters	Values
Particle	Iron ore	Diameter d_p [$\times 10^{-3}$ m]	3–8
		Density ρ_p [kg/m ³]	4865
		Poisson ratio ν_p	0.24
		Shear modulus G_p [gpa]	65
Geometry	Steel surface	Density ρ_g [kg/m ³]	7932
		Poisson ratio ν_g	0.3
		Shear modulus G_g [gpa]	78
		Mesh size d_m [mm]	6.0
Contact	Iron ore/iron ore	Coefficient of restitution $e_{p,d}$	0.45
		Coefficient of static friction $\mu_{s,p,d}$	0.41
		Coefficient of rolling friction $\mu_{r,p,d}$	0.22
		Coefficient of restitution $e_{p,d}$	0.4
	Iron ore/chute	Coefficient of static friction $\mu_{s,p,d}$	0.46
		Coefficient of rolling friction $\mu_{r,p,d}$	0.3
		Particle generation rate q_b [kg/s]	27.78
		Total time [s]	4.0
Simulation	Conditions	Initial horizontal velocity $v_{x,0}$ [m/s]	0.2
		Initial vertical velocity $v_{y,0}$ [m/s]	5.33
		Coefficient of sliding wear α_s [$\times 10^{-13}$ m ² /N]	3.0
		Time step Δt [$\times 10^{-6}$ s]	1.5

**Figure 3.** Sliding wear prediction of a smooth surface of a loading chute.

length of the particle factory is 0.1 m and the width 0.2 m equated to the width of the chute bottom. Furthermore, the particle factory is positioned closely to the area of onset contact between particle and chute. Figure 3 presents the prediction of sliding wear.

Figure 3 shows that the wear areas on the chute surface are divided into three zones. Zone 1 is the curved surface to which severe wear occurs due to the high normal force triggered by the impact of bulk solids. Zone 2 is the curved surface which suffers the sliding wear. Zone 3 is the wear of the straight surface when bulk solids contact the chute end again and travel off. The legend bar denotes the range of the total wear loss for individual meshes through the feeding time. It is also obtained that after 0.5 s steady transport is reached and a steady bulk flow is achieved. The predicted wear rates for the three zones 1–3 are $W_{r,qb,s,1} = 0.97 \times 10^{-13}$ m³/s, $W_{r,qb,s,2} = 1.72 \times 10^{-13}$ m³/s and $W_{r,qb,s,3} = 0.48 \times 10^{-13}$ m³/s, respectively. By repeating this simulation three times, it is demonstrated that the stable wear predictions are achieved.

4.2. Theoretical verification of wear prediction

To verify the effectiveness of sliding wear prediction using the DEM model, theoretical calculation is carried out based on the analytical chute flow model as shown in Figure 1(b). According to Archard (1953), the sliding wear volume by the element mass Δm_b for the distance dl_s is calculated by

$$\Delta W_V, \Delta m_b, s = \alpha_s F_n dl_s \quad (3)$$

in which F_n is the normal force applied on the curved surface of chute bottom. ΔF_b is composed of centrifugal force and gravitational force, i.e.

$$F_n = \Delta m_b \left[\frac{v_s(\theta_L)^2}{R_1} + g_0 \sin \theta_L \right] \quad (4)$$

From Figure 1(b), dl_s is given by,

$$dl_s = R_1 d\theta_L \quad (5)$$

Inserting Equations (4) and (5) into Equation (3), the sliding wear volume by element mass,

$$\Delta W_{V,\Delta m_b,s} = \alpha_s \Delta m_b [v_b(\theta_L)^2 + R_1 g_0 \sin \theta_L] d\theta_L \quad (6)$$

The wear for the element mass Δm_b moving through the curved chute is expressed by the integral of Equation (6) from $\theta_L = \theta_{L,0}$ to $\theta_L = \theta_{L,t}$, where $\theta_{L,0}$ and $\theta_{L,t}$ are chute slope angles corresponding to two boundaries that bulk solids entering and leaving zone 2 (Figure 3). Therefore, the volume of sliding wear on zone 2 caused by element mass Δm_b is,

$$W_{V,\Delta m_b,s} = \alpha_s \Delta m_b \int_{\theta_{L,0}}^{\theta_{L,t}} [v_b(\theta_L)^2 + R_1 g_0 \sin \theta_L] d\theta_L \quad (7)$$

For the total sliding wear of the chute surface ($W_{V,qb,s}$) subjected to the bulk flow rate q_b , it can be estimated by substituting Δm with q_b , i.e.

$$W_{V,qb,s} = \alpha_s \Delta m_b \int_{\theta_{L,0}}^{\theta_{L,t}} [v_b(\theta_L)^2 + R_1 g_0 \sin \theta_L] d\theta_L \quad (8)$$

The velocity of bulk solids subjected to any location θ_L is given as (Roberts 2003),

$$v_b(\theta_L)^2 = \frac{2g_0 R_1}{4\mu_e^2 + 1} [(1 - 2\mu_e^2) \sin \theta_L] + K e^{-2\mu_e \theta_L} \quad (9)$$

where μ_e is equivalent friction factor which combines the coefficient of friction between the bulk solids and the chute surface. μ_e is evaluated by Equation (10) (Roberts 2003),

$$\mu_e = \mu_s (1 + \varpi \frac{H}{B_1}) \quad (10)$$

in which ϖ is estimated at 0.4 corresponding to the condition of transporting a shallow layer of iron ore (Roberts 2003). μ_s is measured at 0.46 (Chen et al. 2017). H is the depth of the bulk solids and B_1 is chute width. Finally, μ_e is calculated at 0.47.

The parameter K in Equation (9) is evaluated by (Roberts 2003),

$$K = \{v_0^2 - \frac{2g_0 R_1}{4\mu_e^2 + 1} [(1 - 2\mu_e^2) \sin \theta_L + 3\mu_e \cos \theta_L]\} e^{2\mu_e \theta_L} \quad (11)$$

Using $v = v_0 = 5.34 \text{ m/s}$ at $\theta = \theta_{L,0} = 28.36^\circ$, it is found that $K = -4.68 \text{ m}^2/\text{s}^2$.

To estimate the wear rate from zone 2, the chute slope angles $\theta_{L,0}$ and $\theta_{L,m}$ are measured at 35.34° and 64.15° , respectively. By inserting K into [Equation \(9\)](#) and integrating [Equation \(8\)](#), the theoretical wear rate for zone 2 is obtained $W_{rqb,s} = 1.68 \times 10^{-10} \text{ m}^3/\text{s}$. By comparing with the DEM prediction $W_{rqb,s,2} = 1.72 \times 10^{-10} \text{ m}^3/\text{s}$, it is demonstrated that the DEM simulation model can correctly predict the sliding wear by iron ore bulk solids.

5. Abrasive wear prediction of bionic surfaces

To predict wear reduction of using the bionic surface of the chute bottom, the geometrical parameters of the bionic model are determined in this section. Besides, the wear of a base case of a bionic surface is predicted and compared to that of a smooth surface. In addition, the sensitivities of geometrical parameters on abrasive wear are investigated.

5.1. Bionic model

[Figure 4](#) illustrates the application of a bionic model (Chen, Schott, and Lodewijks 2017b) to the chute bottom surface, in which the four geometrical parameters a_0 and b_0 are the major and minor radii. c_0 and d_0 are the distances between the centers of convexes, respectively, in vertical and horizontal directions. The determinations of the geometrical parameters of the bionic model are given in the following two paragraphs.

For the geometrical parameters a_0 and b_0 , it is noted that $a_0 > b_0$ such that particles can be transferred along the chute bottom. To enable rolling of particles, the height of the convex is smaller than particle diameter such that b_0 can be determined (i.e. $b_0 < d_{50} = 3.0 \text{ mm}$) (Tong et al. 2007). Due to the fact that smaller sizes of convex results in large number of meshes and thus introducing much simulation time, the minimum size of b_0 is limited to 1.5 mm.

The determinations for c_0 and d_0 are based on similar work by other researchers (Tong et al. 2012; Greiner and Schäfer 2015), in which it shows that c_0 and d_0 can be increased but will give low reduction of wear beyond a range. Thus, in this research c_0 and d_0 are determined when

wear reduction can still be achieved and the simulating time is acceptable. [Table 4](#) lists the values of the four geometrical parameters, in which group 2 is the base case to be applied on chute bottom. Other values are used to investigate the sensitivities of the geometrical parameters ([Section 6](#)).

5.2. Wear prediction of bionic surface

Corresponding to the values of group 2 in [Table 4](#), the DEM predictions of particle velocities for the bionic surface and the smooth surface are shown in [Figure 5](#) (sectional view). It demonstrates that the overall velocities of bulk solids for the bionic surface are lower than those of the smooth surface. Furthermore, it indicates that a portion of particles fly off the chute bottom of the bionic surface, which is ascribed to the fact that particle bounce directions are changed on bionic surface.

In order to estimate material loss because of the bouncing particles, the transport capabilities for the bionic surface and the smooth surface are examined. It demonstrates that the transport capability for bionic surface is lower than smooth surface at initial transport state (before 2.4 s) as a result of the loss from bouncing particles. However, after that time the transport capabilities for both surfaces reach comparable levels. It is noted that although a bionic surface causes certain particles to travel off the chute channel, in practice, such occurrences are restrained. This is because the chute sides are high enough to block flying particles.

To further understand the wear consequences in simulations, the contact pressure on bionic surface and smooth surfaces is compared. It is obtained that the pressure on the bionic surface is less severe than that of the smooth, which implies that the corresponding wear is less severe. The reason can be explained as: the convexes of bionic surface affect directionalities of the transported particles (as is seen in [Figure 5](#)), which results in less interactions between particles

Table 4. Geometrical parameters of the bionic model.

Geometrical parameters	Group 1	Group 2	Group 3	Group 4
Major radius a_0 [mm]	2	3	4	5
Minor radius b_0 [mm]	1.5	2	2.5	3
Vertical distance c_0 [mm]	30	40	50	60
Horizontal distance d_0 [mm]	25	30	35	40

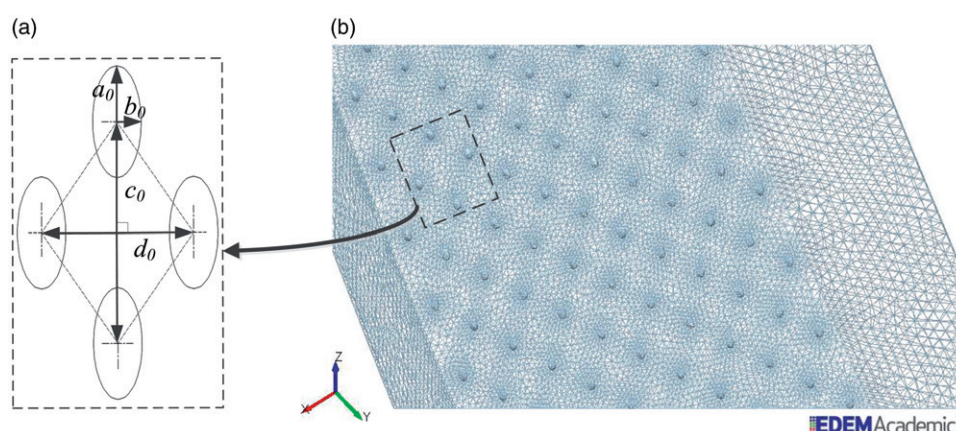


Figure 4. Bionic design of wear resistant surface (a) geometrical parameters; (b) meshed surface of the base case (group 2).

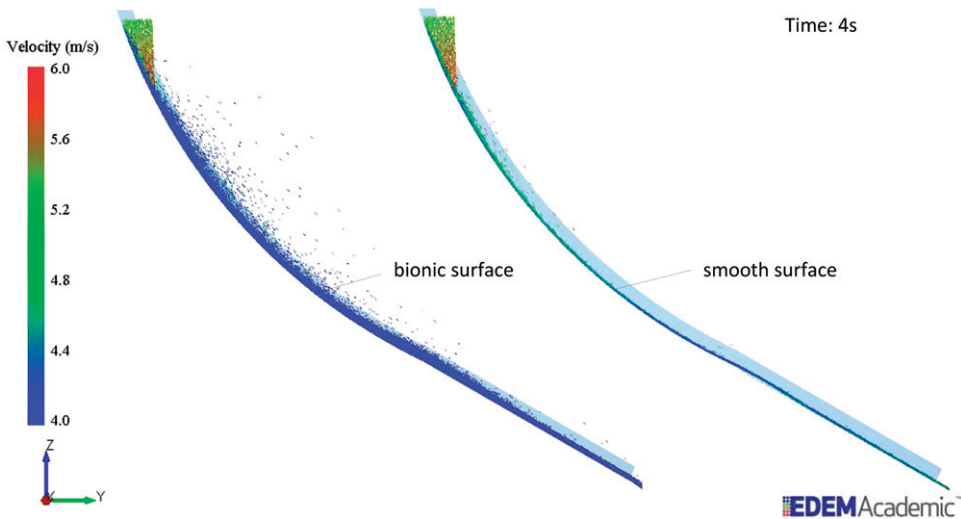


Figure 5. Sectional views of particle velocities for bionic and smooth surfaces (group 2).

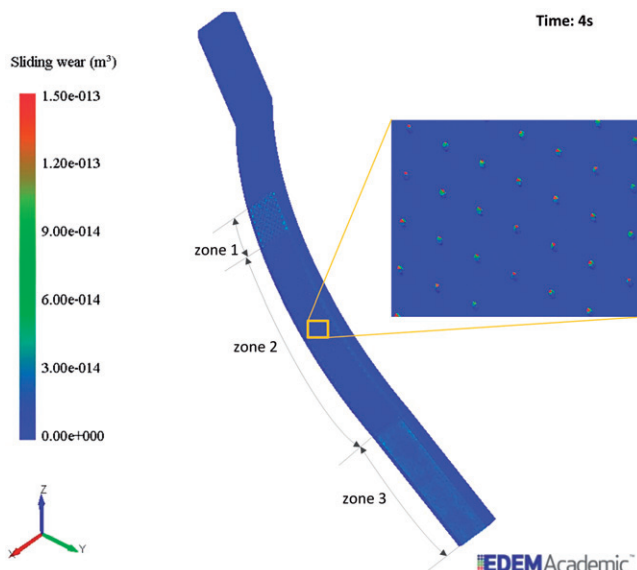


Figure 6. Wear prediction for the base case of a bionic surface (group 2).

and bionic surface and thus having lower contact pressure. By contrast, the pressure on the straight surface near the exit is higher than that of the smooth surface. This is also due to the fact that the convexes change directionalities of particles and can introduce more contact areas with the surface of chute exit.

Figure 6 shows the wear prediction of the bionic surface from the base case (group 2). It can be seen that the bionic surface also exhibits similar wear zones 1–3 as those of the smooth surface. Besides, more wear occurs to convexes than to the matrix part of the chute surface. This is ascribed to the convexes that induce interactions with particles such that less particles wear the matrix part of the chute surface. This phenomenon is consistent with the referred research of resistance reduction by sliding particles (Ren et al. 1995).

To compare wear loss between the bionic surface and smooth surface, their corresponding total wear volumes for zone 2 are compared. It is obtained that both bionic surface and smooth surface initially undergo exponential increase and quickly maintain linear increase, which means that

steady transport status is arrived. For the steady transport status, the bionic surface produces less wear volumes than the smooth surface. The reduction of wear can be quantified by Equation (12):

$$\lambda = \frac{W_{V,s} - W_{V,b}}{W_{V,s}} * 100\% \quad (12)$$

in which λ is designated as the ratio of wear reduction; $W_{V,s}$ and $W_{V,b}$ are wear volumes with respect to smooth surface and bionic surface. By using the predicted wear volumes from 1.6 to 2.4 s, the ratio of wear reduction is calculated at 30.7%.

6. Sensitivity analysis of bionic model

The previous section has demonstrated the abrasive wear reduction of a bionic surface compared to smooth surface. To investigate the influences of varying four geometrical parameters (a_0 , b_0 , c_0 and d_0) on wear reduction, a sensitivity study is performed. Using the values given in Table 4, the Figures 7–10 present the wear volumes of bionic surfaces subjected to the four geometrical parameters. In each figure, the wear of a smooth surface is also incorporated for comparisons.

Figure 7 illustrates the wear volumes of the four bionic surfaces subjected to four values of the major radius (a_0). In general, the wear volumes increase with increasing major radius a_0 . Notably, a significant increase occurs when increasing a_0 = 2 mm to 3 mm. Nevertheless, this increase in wear volume becomes less significant when $a_0 > 3$ mm. The reason for this is that the contact between particle and convex is more isotropic for a_0 = 2 mm which corresponds to hemispherical convex. This can maximally increase the contact directionality (Ren et al. 1995; Greiner and Schäfer 2015) and thus enabling the highest reduction of wear (43%). With further increasing a_0 , the convexes tend to be ellipsoidal and thus the directionality reduces.

Figure 8 presents the wear volumes for the four bionic surfaces with respect to changing minor radius (b_0). It shows that a steady and significant wear reduction is obtained with increasing the minor radius. Thus, varying minor

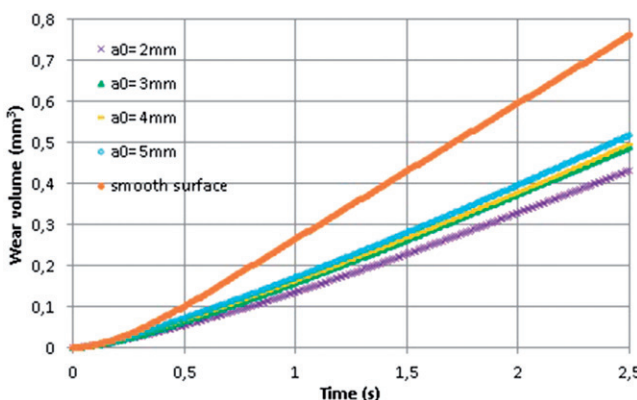


Figure 7. Wear volume as a function of major radius a_0 .

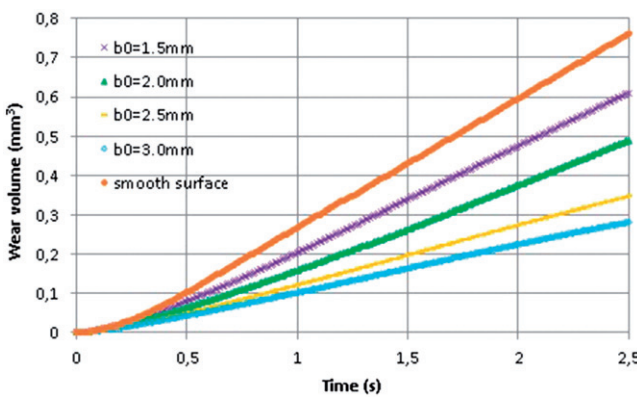


Figure 8. Wear volume as a function of minor radius b_0 .

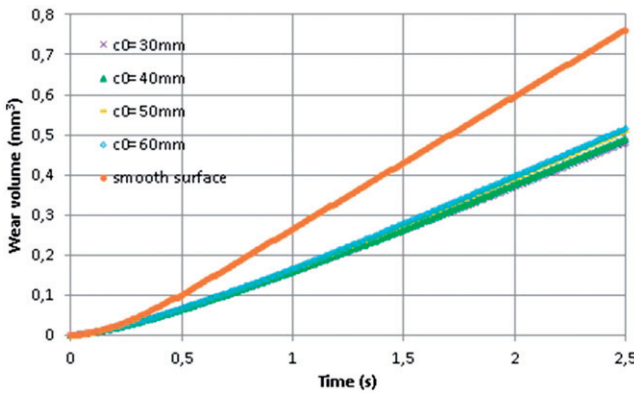


Figure 9. Wear volume as a function of vertical distance c_0 .

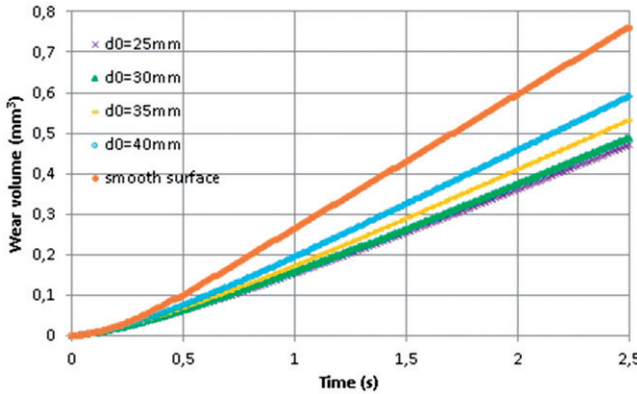


Figure 10. Wear volume as a function of transverse distance d_0 .

radius exhibits very sensitive effects on the wear. The reason is that with increasing the minor radius, the shape of semi-ellipsoidal convex tends to be hemispherical (i.e. a_0/b_0 is increasing to 1.0). The hemispherical shape is beneficial to increasing contact as the cases for major radius $a_0 = 2$ mm. For the group of the values for b_0 , the maximum reduction of the wear prediction is obtained at 63% for $b_0 = 3$ mm.

Figure 9 shows the wear volumes for the bionic surfaces by varying vertical distance (c_0), in which a minor increase of wear is observed for $c_0 = 30$ to 60 mm. It demonstrates that this parameter is not very sensitive on the wear prediction for the test range. The reason is that when c_0 is much larger than particle sizes (i.e. $c_0 > 3d_p$), increasing c_0 promotes little influences on increasing contact directionality (Tong et al. 2007, 2012). Thus, among the four values for c_0 the maximal wear reduction is 37% for $c_0 = 30$ mm.

Figure 10 provides the wear volumes with respect to the horizontal distance d_0 . It is seen that the wear volume increases with increasing horizontal distance d_0 . This indicates that for the horizontal distance $d_0 > 3d_p$ the contact directionality decreases by increasing d_0 . Moreover, it shows that the larger the d_0 , the faster the increase of wear volume. At $d_0 = 25$ mm, the highest ratio of wear reduction is calculated at 38%.

In summary, the minor radius a_0 is the most sensitive parameter whilst vertical distance c_0 the least. The wear volumes of all bionic surfaces are lower than that of smooth surface. The maximum reduction of wear is achieved when the convex becomes semi-hemispherical (i.e. $a_0/b_0 = 1$). This provides valuable reference for the design of bionic surface for the bulk solids handling equipment.

7. Conclusions

This paper presented the DEM simulations of the abrasive wear reduction of bulk solids handling equipment using bionic surface. Four conclusions are drawn as follows:

1. Using the determined DEM values, the sliding wear volume is accurately predicted with respect to steady transport of iron ore.
2. In comparison with a conventional smooth surface, the abrasive wear reduction of a bionic surface of a transfer chute bottom is demonstrated.
3. The effects on wear reduction subjected to varied geometrical parameters of the bionic model are obtained and the maximum reduction of wear is 63%.
4. This research provides important reference for designing bionic surface for the abrasive wear reduction of bulk solids handling equipment.

Nomenclature

Latin letters

a_0	major radius of the bionic model [mm]
b_0	minor radius of the bionic model [mm]
c_0	long diagonal of the bionic model [mm]

C_n	coefficient of damping force [N]
d_0	short diagonal of the bionic model [mm]
d_p	particle diameter [mm]
d_m	geometry mesh size [mm]
e	coefficient of restitution [dimensionless]
F_d	drag force for Δm_b [N]
F_r	reaction force for Δm_b [N]
F_n	normal force for Δm_b [N]
g_0	gravitational acceleration [m^2/s^2]
G	shear modulus [GPa]
i	number of wear events [dimensionless]
K	parameter for estimating flow velocity at any slope angle [m^2/s^2]
l_s	sliding distance made by the particle [m]
q_b	iron ore feeding rate [kg/s]
S	stiffness [N/m]
Δt	time step [s]
T	time [s]
v	relative velocity [m/s]
W_V	total wear loss in volume [m^3]
W_{V0}	wear loss in volume from one geometry mesh [m^3]
$W_{qb,s}$	the total sliding wear volume on the chute surface [m^3]

Roman letters

α_s	coefficient of sliding wear [m^2/N]
δ	contact overlap [m]
$\Phi_{1,2,3}$	angles for characterizing bulk flow [$^\circ$]
γ	angle between chute bottom and chute side [$^\circ$]
μ_e	equivalent friction factor [dimensionless]
μ_s	coefficient of static friction [dimensionless]
μ_r	coefficient of rolling friction [dimensionless]
λ	rate of wear reduction [dimensionless]
ω	rotating speeds [$^\circ/s$]
ϱ	density of the chute equipment surface [kg/m^3]
ϖ	pressure ratio [dimensionless]
θ_L	chute slope angle measured from gravitational direction [$^\circ$]
θ_w	wall friction angle between Sishen iron ore and steel surface [$^\circ$]
Ψ	chute cut-off angle [$^\circ$]

Disclosure statement

No potential conflict of interest was reported by the authors.

Funding

The authors are grateful for the funding from China Scholarship Council (No. 201206170158). In addition, the first author would like to give thanks to the New Teacher Research Seed Fund of NUAA (No. 1011/90YAH18012).

ORCID

Gabriel Lodewijks  <http://orcid.org/0000-0002-6466-4346>

References

- ANSYS Inc. 2016. ANSYS Workbench 16.2: Mesh-Meshing. Pennsylvania: Academic Research.
- Archard, J. F. 1953. Contact and rubbing of flat surfaces. *Journal of Applied Physics* 24 (8):981–8. doi:[10.1063/1.1721448](https://doi.org/10.1063/1.1721448).
- Barrios, G. K. P., R. M. de Carvalho, A. Kwade, and L. M. Tavares. 2013. Contact parameter estimation for DEM simulation of iron ore pellet handling. *Powder Technology* 248:84–93. doi:[10.1016/j.powtec.2013.01.063](https://doi.org/10.1016/j.powtec.2013.01.063).
- Boemer, D., and J. P. Ponthot. 2017. A generic wear prediction procedure based on the discrete element method for ball mill liners in the cement industry. *Minerals Engineering* 109:55–79. doi:[10.1016/j.mineng.2017.02.014](https://doi.org/10.1016/j.mineng.2017.02.014).
- Chen, G., D. L. Schott, and G. Lodewijks. 2017a. Sensitivity analysis of DEM prediction for sliding wear by single iron ore particle. *Engineering Computations* 34 (6):2031–53.
- Chen, G., D. L. Schott, and G. Lodewijks. 2017b. Bionic design methodology for wear reduction of bulk solids handling equipment. *Particulate Science and Technology* 35 (5):525–32. doi:[10.1080/02726351.2016.1144666](https://doi.org/10.1080/02726351.2016.1144666).
- Chen, G., Y. Liu, G. Lodewijks, and D. L. Schott. 2017. Experimental research on the determination of the coefficient of sliding wear under iron ore handling conditions. *Tribology in Industry* 39 (3): 378–90. doi:[10.24874/ti.2017.39.03.13](https://doi.org/10.24874/ti.2017.39.03.13).
- Cundall, P. A., and O. D. L. Strack. 1979. A discrete numerical model for granular assemblies. *Geotechnique* 29 (1):47–65.
- DEM Solutions Ltd. 2016a. EDEM 2.6 Theory Reference Guide. Edinburgh: DEM Solutions Ltd.
- DEM Solutions Ltd. 2016b. EDEM 2.7 User Guide. Edinburgh: DEM Solutions Ltd.
- Derakhshani, S. M., D. L. Schott, and G. Lodewijks. 2016. Calibrating the microscopic properties of quartz sand with coupled CFD-DEM framework. *Engineering Computations* 33 (4):1141–60. doi:[10.1108/MRR-09-2015-0216](https://doi.org/10.1108/MRR-09-2015-0216).
- Greiner, C., and M. Schäfer. 2015. Bio-inspired scale-like surface textures and their tribological properties. *Bioinspiration & Biomimetics* 10 (4):044001. doi:[10.1088/1748-3190/10/4/044001](https://doi.org/10.1088/1748-3190/10/4/044001).
- Grima, A. P., and P. W. Wypych. 2011. Investigation into calibration of discrete element model parameters for scale-up and validation of particle-structure interactions under impact conditions. *Powder Technology* 212(1):198–209. doi:[10.1016/j.powtec.2011.05.017](https://doi.org/10.1016/j.powtec.2011.05.017).
- Hilgraf, P. 2007. Wear in bulk materials handling. *Bulk Solids Handling* 27 (7):464–77.
- Khanal, M., and R. Morrison. 2009. DEM simulation of abrasion of nonspherical particles in tumbling mill. *Particulate Science and Technology* 27 (1):68–76. doi:[10.1080/02726350802611853](https://doi.org/10.1080/02726350802611853).
- Lumay, G., F. Boschini, K. Traina, S. Bontempi, J. C. Remy, R. Cloots, and N. Vandewalle. 2012. Measuring the flowing properties of powders and grains. *Powder Technology* 224:19–27. doi:[10.1016/j.powtec.2012.02.015](https://doi.org/10.1016/j.powtec.2012.02.015).
- Malshe, A., K. Rajurkar, A. Samant, H. N. Hansen, S. Bapat, and W. Jiang. 2013. Bio-inspired functional surfaces for advanced applications. *CIRP Annals - Manufacturing Technology* 62 (2):607–28. doi:[10.1016/j.cirp.2013.05.008](https://doi.org/10.1016/j.cirp.2013.05.008).
- Müller, F. A., C. Kunz, and S. Gräf. 2016. Bio-inspired functional surfaces based on laser-induced periodic surface structures. *Materials* 9 (6):476. doi:[10.3390/ma9060476](https://doi.org/10.3390/ma9060476).
- Popov, V. L. 2010. *Contact mechanics and friction: Physical principles and applications*. Heidelberg, Dordrecht, London, New York: Springer.
- Powell, M. S., N. S. Weerasekara, S. Cole, R. D. LaRoche, and J. Favier. 2011. DEM modelling of liner evolution and its influence on grinding rate in ball mills. *Minerals Engineering* 24 (3–4):341–51. doi:[10.1016/j.mineng.2010.12.012](https://doi.org/10.1016/j.mineng.2010.12.012).
- Ren, L., J. Tong, S. Zhang, and B. Chen. 1995. Reducing sliding resistance of soil against bulldozing plates by unsmoothed bionics surfaces. *Journal of Terramechanics* 32 (6):303–9.
- Roberts, A. W. 2003. Chute performance and design for rapid flow conditions. *Chemical Engineering & Technology* 26 (2):163–70. doi:[10.1002/ceat.200390024](https://doi.org/10.1002/ceat.200390024).
- Sartori, J., U. Pal, and A. Chakrabarti. 2010. A methodology for supporting ‘transfer’ in biomimetic design. *Artificial Intelligence for Engineering Design, Analysis and Manufacturing* 24 (4):483–506. doi:[10.1017/S0890060410000351](https://doi.org/10.1017/S0890060410000351).
- SCRIBD. 2017. Acrylic Material Data (from PARSGLASS). <https://www.scribd.com/mobile/doc/8637812/Acrylic-Material-Data-from-PARSGLASS#>. (accessed October 17, 2016).

- Tang, H., X. Zhang, and S. Ji. 2017. Discrete element analysis for shear band modes of granular materials in triaxial tests. *Particulate Science and Technology* 35 (3):277–14. doi:[10.1080/02726351.2016.1153547](https://doi.org/10.1080/02726351.2016.1153547).
- Tong, J., L. Tie Biao, M. Yun Hai, W. Heng Kun, R. Lu Quan, and R. D. Arnett. 2007. Two-body abrasive wear of the surfaces of pangolin scales. *Journal of Bionic Engineering* 4 (2):77–84. doi:[10.1016/S1672-6529\(07\)60017-1](https://doi.org/10.1016/S1672-6529(07)60017-1).
- Tong, J., Z. Zhang, Y. Ma, D. Chen, B. Jia, and C. Menon. 2012. Abrasive wear of embossed surfaces with convex domes. *Wear* 274–275:196–202. doi:[10.1016/j.wear.2011.08.027](https://doi.org/10.1016/j.wear.2011.08.027).
- Vincent, J. F. V. 2009. Biomimetics – a review. *Proceedings of the Institution of Mechanical Engineers, Part H: Journal of Engineering in Medicine* 223 (8):919–39. doi:[10.1243/09544119-jeim561](https://doi.org/10.1243/09544119-jeim561).